
Beta Dose Point Kernels for Radionuclides of Potential Use in Radioimmunotherapy

William V. Prestwich, Josane Nunes, and Cheuk S. Kwok

Department of Physics, McMaster University, and Hamilton Regional Cancer Centre, Ontario Cancer Foundation, Hamilton, Ontario, Canada

Beta dose point kernels for ^{32}P , ^{67}Cu , ^{90}Y , ^{131}I , ^{186}Re , and ^{188}Re nuclides appropriate for radioimmunotherapy are calculated based upon Monte Carlo results. The calculations are shown to differ significantly from values based upon solutions to the electron transport equation. Agreement with experiment for ^{32}P is found to be improved for the former as compared with the latter. Values of the scaled dose point kernels are tabulated at 4% intervals of the continuous slowing down approximation range for each of the six radionuclides. Beta dose distributions are also tabulated at corresponding distances from the source. This data may be used to calculate the spatial dose distribution expected following administration of radiolabeled monoclonal antibodies, aiding in optimum selection of the appropriate radionuclide. Parameters for functions providing analytic representation of the calculated scaled dose point kernels of individual beta groups are presented.

J Nucl Med 30:1036-1046, 1989

There is currently active investigation of the application of labeled monoclonal antibodies to radioimmunotherapy (1). Administration of labeled antibody should lead to a concentration of radioactivity at specific tumor sites as the antibody attaches to the target antigen. This behavior produces a highly nonuniform spatial distribution of activity in the subject. In most situations involving internal dosimetry the assumption of spatial uniformity is made, thereby justifying the use of equilibrium doses. The nonuniformity expected in radioimmunotherapy invalidates such an approach for this procedure, producing instead a nonuniform spatial dose distribution arising from emitted beta particles. This is precisely the objective sought in order to maximize discrimination between affected and healthy tissue.

Treatment planning requires estimation of the dose distribution, given that the activity distribution may be measured using imaging techniques, or otherwise inferred. Calculation of the beta dose distribution from the activity distribution is only straightforward if the medium is homogeneous with regard to electron transport properties. While this approximation probably is

justified for soft tissues, it is not for bone and air interfaces.

In the homogeneous situation, the principle of linearity ensures that once the dose distribution from a unit point source is established, then the dose may be calculated for any activity distribution. The beta dose distribution about a unit point source of the radioisotope of interest is referred to as the beta dose point kernel. It is this quantity which is the subject of consideration in this work.

Extensive tabulations of beta dose point kernels have been published elsewhere (2), but these do not include the effects of energy fluctuations. We report here on calculations of dose point kernels that do include such effects. The results are compared both with the previously tabulated values and indirectly with experiment. The nuclides chosen are those which are potential candidates for application to radioimmunotherapy. These are ^{32}P , ^{67}Cu , ^{90}Y , ^{131}I , ^{186}Re , and ^{188}Re .

Finally, parameters suitable for analytic representation of the calculated dose point kernels are presented. The accuracy of the representation is also discussed.

THEORETIC BACKGROUND

Scaled Dose Point Kernel in Continuous Slowing Down Approximation

As an extremely oversimplified model, consider a monoenergetic isotropic point source emitting electrons which move

Received Aug. 15, 1988; revision accepted Jan. 5, 1989.

For reprints contact: C. S. Kwok, PhD, Hamilton Regional Cancer Centre, Ontario Cancer Foundation, 711 Concession St., Hamilton, Ontario, L8V 1C3, Canada.

W. V. Prestwich, PhD, Dept. of Physics, McMaster University, Hamilton, Ontario, L8S 4K1, Canada.

radially outward and slow down continuously according to a stopping power function $S(E)$. If the source energy is E_0 , the electron energy at a distance r from the origin, at which the source is located, is given by

$$r = \int_{E(r)}^{E_0} \frac{dE}{S(E)} \quad (1)$$

The continuous slowing down approximation (CSDA) range then satisfies

$$r_0 = \int_0^{E_0} \frac{dE}{S(E)} \quad (2)$$

The absorbed dose per source transformation is then

$$D(r) = \frac{S(E(r))}{4\pi\rho r^2} \quad (3)$$

The specific absorbed fraction is given by

$$\Phi(r, E_0) = \frac{S(E(r))}{4\pi\rho r^2 E_0} \quad (4)$$

This quantity satisfies the constraint

$$\int_0^\infty 4\pi\rho r^2 \Phi(r, E_0) dr = 1. \quad (5)$$

It is convenient to introduce a dimensionless quantity to represent distance as the fraction of the CSDA range, designated

$$x = r/r_0. \quad (6)$$

Defining a scaled electron dose point kernel through the relation

$$F(x, E_0) = 4\pi\rho r_0^2 \Phi(r, E_0) \quad (7)$$

introduces a quantity satisfying

$$\int_0^\infty F(x, E_0) dx = 1. \quad (8)$$

For the simplified model leading to Equation (4), the scaled point kernel becomes

$$F(x, E_0) = \frac{r_0 S(E(x, r_0))}{E_0} = S(E(x, r_0)) / \langle S \rangle = 0 \quad x \geq 1. \quad (9)$$

In Equation (9) the track average stopping power

$$\langle S \rangle = E_0/r_0 \quad (10)$$

has been introduced. It then becomes possible to interpret the scaled point kernel as the ratio of the stopping power at a particular point along the electron track to the average stopping power over the entire track.

Of course neither the assumption of straight-line motion nor that of continuous energy loss is justified for electron transport. The treatment does, however, illustrate the physical basis of the scaled dose point kernel as the ratio of an energy loss function to the track average stopping power.

Monoenergetic Dose Point Kernels

The departure from straight-line motion was first taken into account in detail by Spencer (3) who numerically solved

the transport equation in the CSDA taking into account multiple scattering. The calculations used the method of moments, and yielded the energy dissipation function for a carbon medium,

$$J(x, E_0) = \frac{E_0 F(x, E_0)}{r_0 S(E_0)}. \quad (11)$$

Again, in the extreme straight-ahead approximation used for Equation (4), the energy dissipation function becomes the ratio of the stopping power at the distance $r = xr_0$ to the stopping power at the origin. The dose point kernels and the energy dissipation function obtained in this approach both vanish for $x \geq 1$ corresponding to distances greater than the CSDA range.

An important advance has been the development of Monte Carlo methods by Berger (4) specifically designed to simulate electron transport. By dividing the electron path into small segments and making use of the angular and energy distribution data from thin foil experiments, Berger was able to take into account both multiple scattering and energy loss fluctuations. Departures from continuous slowing down resulting from delta-ray and bremsstrahlung production were also incorporated. These methods have been applied to the calculation of monoenergetic dose point kernels for 36 energies ranging from 0.5 keV to 10 MeV (5).

The monoenergetic dose point kernels calculated by Monte Carlo simulation differ in two respects from those based on numerical solution of the transport equation. First, because of energy loss straggling, some energy is transported to distances greater than the CSDA range. The calculations indicate a maximum penetration up to $x = 1.2$. Second, the scaled dose-point kernels no longer exactly satisfy the unit area constraint in Equation (8) because of electron-photon conversion in radiative stopping. The area in this case is reduced by the radiative yield, that amounts to 1.7% at 4 MeV. In the energy range below 2.5 MeV the area constraint is satisfied to better than 1% so that Equation (8) may be considered to hold in practice in this case.

The dose point kernels calculated by the two methods for 1 MeV electrons are compared in Figure 1. The influence of energy loss fluctuations included in the Monte Carlo simulation results in a more dispersive dose distribution. Since both areas are essentially unity, the increased dose near the CSDA range that is produced by these fluctuations is balanced by a decrease in dose near the origin. Because the scaled point kernels are decreasing sharply in value near $x = 1$, the relative dose increase here is much greater than the relative depression near $x = 0$. For example, the ratio of the dose point kernel with energy loss fluctuations to that without is 5.5 at $x = 0.9$ and 0.91 at $x = 0$. Clearly this implies that the neglect of such fluctuations results in significant underestimates of dose near the end of the electron range.

At the origin, the scaled dose point kernel obtained from Spencer's calculation coincides with the simplified model so that Equation (9) may be applied to give

$$F(0, E_0) = r_0 S(E_0)/E_0. \quad (12)$$

The ratio of the Monte Carlo results at $x = 0$ to that given by Equation (12) are plotted in Figure 2 as a function of the electron energy. Above 0.5 MeV the dose reduction ranges from 6% to 12%. Below 50 keV the dose reduction is again

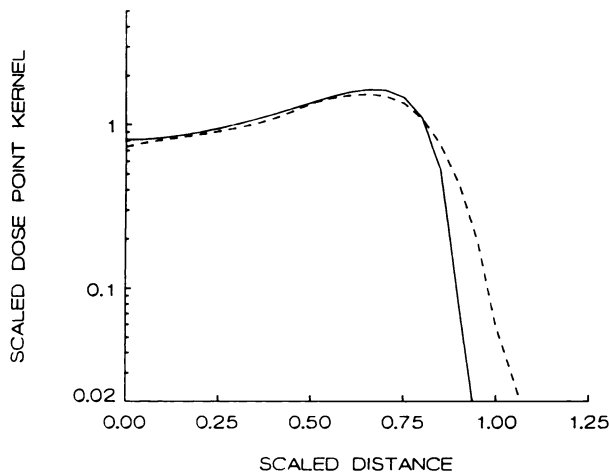


FIGURE 1
Comparison between the 1-MeV dose point kernels calculated from the transport equation (—) and by Monte Carlo methods (---). The latter is more disperse, extending to larger distances, while being slightly lower in value in the near region.

in excess of 6%. The curve peaks near 0.15 MeV, at which point the reduction factor is only about 2%. The energy averaged reduction factor calculated over the range 0.01 MeV to 3 MeV is 9.4%.

Radionuclide Beta Dose Point Kernels

For a beta-emitting radionuclide it is necessary to calculate the dose point kernel which results from a spectrum of electrons. The spectrum associated with beta-decay may in general be written

$$n(E) = \sum_{i=1}^N \beta_i n_i(E) \quad (13)$$

representing a decomposition into N groups, each of which has a branching probability of β_i and end-point energy E_i . Also

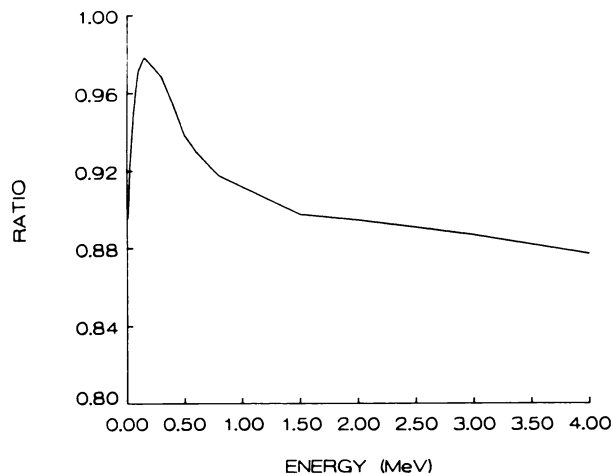


FIGURE 2
Variation of the ratio of the Monte Carlo dose point kernel to the transport kernel at the origin with electron energy.

associated with each group is an average energy

$$\langle E_i \rangle = \int_0^{E_i} E n_i(E) dE \quad (14)$$

given that the spectral distribution $n_i(E)$ is normalized to unit area.

The specific absorbed fraction associated with the i^{th} beta-group is then given by

$$\Phi_i(r) = \int_0^{E_i} \frac{E_0}{\langle E_i \rangle} n_i(E_0) \Phi(r, E_0) dE_0. \quad (15)$$

From Equation (7) it follows that

$$4\pi\rho r^2 \Phi_i(r) = \int_0^{E_i} \frac{E_0}{r_0 \langle E_i \rangle} n_i(E_0) F\left(\frac{r}{r_0}, E_0\right) dE_0. \quad (16)$$

A scaled dose point kernel for a beta group may also be introduced. To this end a scaled distance is defined as the fraction of the CSDA range for an electron with energy E_i . Designating the latter r_i , then the scaled dose point kernel for the i^{th} beta group becomes

$$F_i(x) = 4\pi\rho r^2 r_i \Phi_i(r), \quad (17)$$

where $x = r/r_i$. Scaling the distance in this manner differs from that suggested by Berger (6), who uses the 90% point. It has the advantage, however, of using a quantity that is more readily available, the CSDA range.

The specific absorbed fraction associated with the complete beta spectrum of the isotope may then be determined from the relation

$$4\pi\rho r^2 \Phi_\beta(r) = \sum_{i=1}^N \beta_i \frac{\langle E_i \rangle}{r_i} F_i\left(\frac{r}{r_i}\right) / \sum_{i=1}^N \beta_i \langle E_i \rangle. \quad (18)$$

A scaled dose point kernel for this quantity may also be defined through the equation

$$F_\beta(x) = 4\pi\rho r^2 r_N \Phi_\beta(r), \quad (19)$$

where $x = r/r_N$ and r_N is the CSDA range for the highest energy beta group in the decay scheme of the radioisotope. Since the specific absorbed fraction is the ratio of dose to average beta energy, then $F_\beta(x)$ can be related to the dose distribution tabulated by Cross (2) by calculating

$$r^2 D(r) = k \sum_{i=1}^N \beta_i \langle E_i \rangle F_\beta\left(\frac{r}{r_N}\right) / r_N, \quad (20)$$

where $k = 45.84$ is a conversion factor relating $\text{MeV cm}^2 \text{g}^{-1}$ per transformation to $\text{mGy cm}^2 \text{MBq}^{-1} \text{hr}^{-1}$.

The calculation indicated in Equation (15) requires knowledge of the spectral distribution $n_i(E)$. This function is determined by the end-point energy E_i , the atomic number of the daughter nucleus Z , and the angular momentum transfer in the decay process. A more explicit description of the function and approximations used in this work for its evaluation are given in the appendix.

COMPUTATIONAL PROCEDURES

Representation of Monoenergetic Dose Point Kernels

The surface generated from the scaled monoenergetic dose point kernels, derived by Monte Carlo techniques, was represented using bicubic splines. The algorithm employed, named

SMOOPY, was developed by Dierckx (7). The routine achieves smoothness by minimizing the sum of squares of discontinuities of third-order derivatives at interior knots, while selecting knots to satisfy a goodness of fit constraint. The latter is based upon an upper bound on the sum of squared residuals referred to as the smoothing factor. The code was modified to include weighting to improve the representation in the region in which the data approach zero. This was accomplished by assigning the equivalent of standard deviations to the data such that the weight of the zero values was greater by a factor of nine than that for nonzero values. The representation produced by the spline coefficients was found to undergo small negative excursions in the region of zero values. The representation was modified by a logical condition to set all negative values to zero.

Typical dose point kernels generated in this manner are compared with the input data in Figures 3 to 5. The input data file consisted of 775 values. It is difficult to quantify simply the goodness of the fit in terms of the relative deviation, because of the existence of zero values. An average relative deviation was calculated from the ratio of the average root mean square deviation to the average value of the data and found to be 0.25%. As might be expected, the largest relative deviations occur as the function approaches zero. An alternative description of the overall quality of the fit can be made in terms of the absolute deviation, bearing in mind that the data values range from 0 to 1.72. The fraction of all data with s.d.s < 0.001, 0.003, and 0.02 is 66%, 91%, and 100%, respectively. The lowest energy included in the surface is 0.5 keV. The dose-point kernel was assumed to have the same shape as that at 0.5 keV for all lower energy electrons.

The bicubic spline representation is superior to the analytic representation of monoenergetic dose point kernels investigated earlier (8). In the latter case there was a tendency to underestimate the tabulated values for the region $x > 0.9$ and $E > 0.5$ MeV.

Calculation of CSDA Range

As indicated in Equation (16), calculation of the beta dose point kernel requires the evaluation of the CSDA range. To

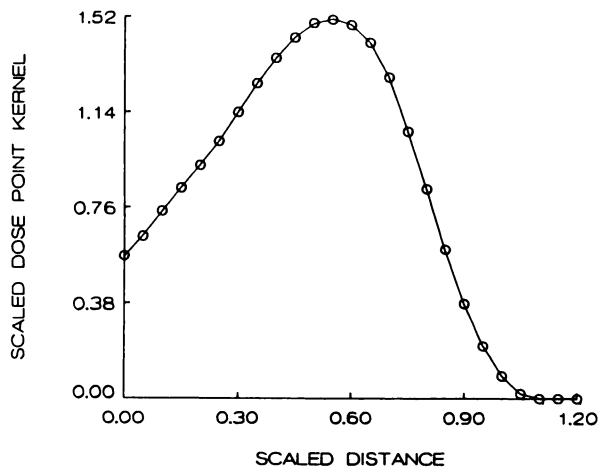


FIGURE 3
Comparison between the spline representation (—) and Monte Carlo values for the 2-keV monoenergetic dose point kernel. The latter are indicated as circles.

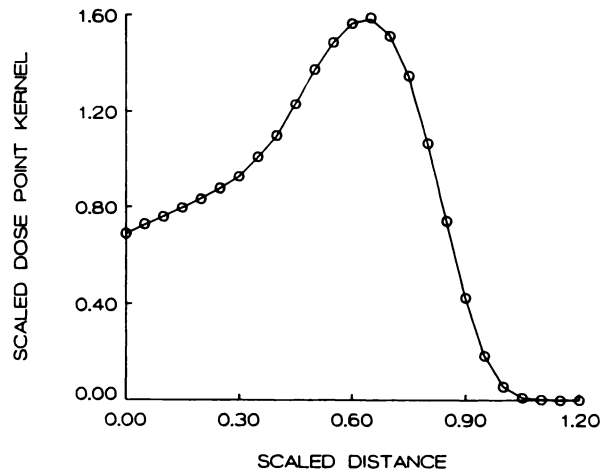


FIGURE 4
Spline representation for the 0.6-MeV electron dose point kernel.

accomplish this task approximating formulae have been developed. For the region between 10 keV and 2.5 MeV a modified power law described previously (8) has been used to represent the data tabulated by Berger and Seltzer (9). This formula fits the data to better than 1.5%. For the region from 0.5 keV to 10 keV the data of La Verne et al. (10) were used. These data had to be fitted in sections. For the region from 1 keV to 10 keV a simple second order polynomial in energy was used. For the region between 0.05 keV and 0.5 keV a third order polynomial was used. In the region from 0.5 keV to 1 keV the range was calculated as the weighted average of values calculated by extrapolation of the two formulae, insuring a continuous joining of the two regions. The quality of the fit is illustrated in Figure 6. The largest deviation from the data occurs at 1 keV and is 5%. Details are given in the appendix.

Calculation of Beta Spectra

As discussed by Dillman (11) the expression for an allowed beta spectrum involves the complex gamma function. We

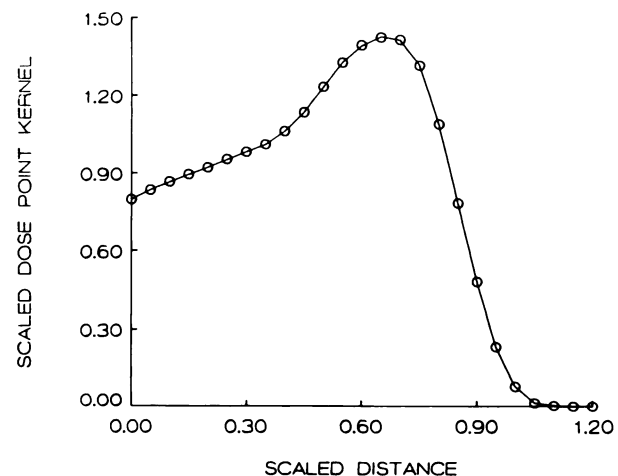


FIGURE 5
Spline representation for the 2-MeV electron dose point kernel.

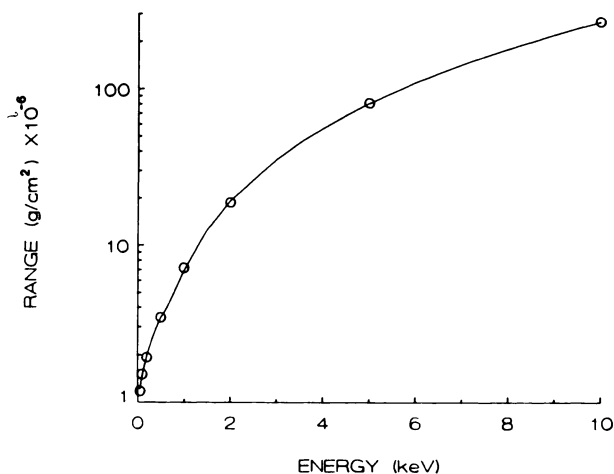


FIGURE 6
Fitted curve (—) for the low-energy CSDA range data. The curve is derived from equations A15 and A16. Circles are data from Ref. (10).

have developed a simple modified approximation, described in the Appendix, thereby avoiding the computation of this function. Comparison with the exact expression indicates agreement to within 0.6% for electron energies up to 3 MeV and for atomic numbers up to 100, encompassing the entire range of potential radioisotopes. Since the beta transitions corresponding to the ^{90}Y decay and the 0.81 MeV group in iodine-131 (^{131}I) are first-forbidden unique, estimation of the corresponding shape factors is required. An approximate description of this quantity has also been developed and is described in more detail in the appendix. The approximation reproduces the tabulated values (12) to within 0.4% for these beta transitions. A comparison between the approximate shape factor and that obtained from the tables is given in Figure 7 for ^{131}I .

In performing the calculation of Equation (16), an energy

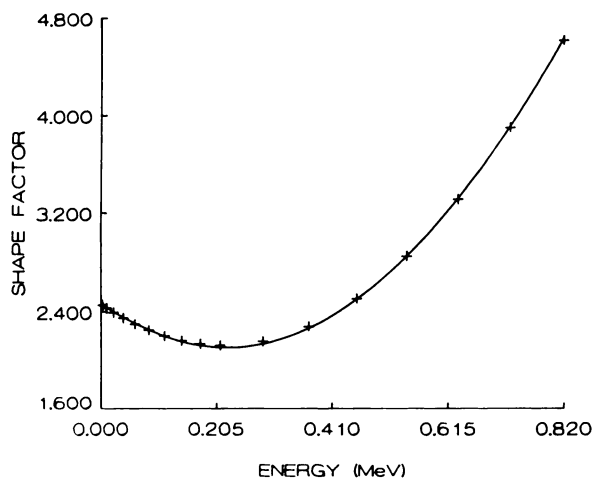


FIGURE 7
Approximation of the shape factor for the first-forbidden unique transition in ^{131}I . The calculated values (+) are based on published tables, while the curve follows from equations A12–A14.

group structure was imposed upon the continuous beta spectrum, giving the discrete spectrum

$$n_i(E) = \sum_{n=1}^M n_i(\epsilon_n) \cdot \delta(E - \epsilon_n). \quad (21)$$

In the above equation the group energy is

$$\epsilon_n = \left(n - \frac{1}{2} \right) E_i / M, \quad (22)$$

where E_i is the endpoint energy and

$$\sum_{n=1}^M n_i(\epsilon_n) = 1. \quad (23)$$

The sensitivity of the calculated dose point kernel to the choice of M was investigated and found to be highest at the origin. The effect is illustrated in Figure 8 for three typical cases. The sensitivity analysis was performed by calculating the variation with M^{-1} . The asymptotic limit was estimated by fitting the linear portion of the variation and extrapolating to $M^{-1} = 0$. The value obtained for $M = 500$ is within 1% of the asymptote and was adopted for the calculations presented here.

RESULTS

Numeric Dose Point Kernels

Beta dose point kernels were calculated using the branching ratios (13) and endpoint energies (14) summarized in Table 1. Also given in the table are the CSDA ranges at the endpoint energy and the average energy for each beta group. The latter are all in agreement with the values quoted in ICRP38 (13) to within 1.5%.

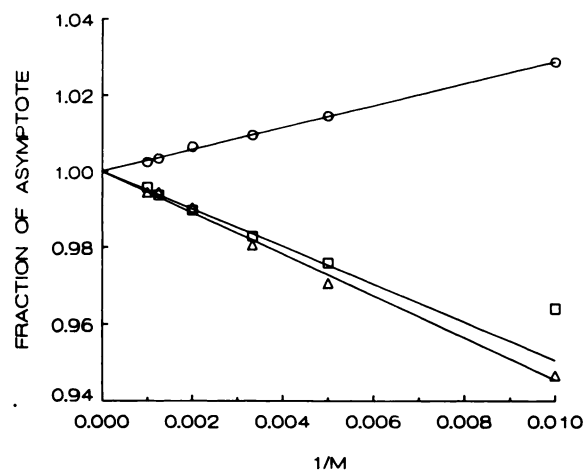


FIGURE 8
Sensitivity of the calculation of the beta dose point kernel to the energy spectrum group structure. M is the number of energy groups used to approximate the continuous spectrum. Data are shown for three examples: the 0.1835-MeV transition in ^{67}Cu (circles), the 1.0715-MeV transition in ^{186}Re (triangles), the 2.12-MeV transition in ^{188}Re (squares). Solid lines are least squares fit to the linear region of the variation.

TABLE 1
Summary of Nuclide Parameters

Isotope	Endpoint Energy (MeV)	Branching Ratio	Range (g/cm ²)	Average Energy (MeV)
³² P	1.708	1.000	0.831	0.694
⁶⁷ Cu	0.184	0.0113	0.039	0.051
	0.395	0.572	0.125	0.122
	0.484	0.216	0.168	0.155
	0.577	0.200	0.215	0.190
⁹⁰ Y	2.286	1.000	1.13	0.938
¹³¹ I	0.248	0.0213	0.062	0.069
	0.304	0.0062	0.085	0.087
	0.334	0.0736	0.098	0.097
	0.606	0.894	0.230	0.192
	0.807	0.0042	0.337	0.284
¹⁸⁶ Re	0.934	0.21	0.407	0.308
	1.072	0.73	0.483	0.362
¹⁸⁸ Re	1.487	0.016	0.712	0.531
	1.965	0.251	0.966	0.735
	2.120	0.716	1.046	0.803

The resulting scaled beta dose point kernels are given in Table 2. These quantities provide information regarding the intrinsic shape of the function. Absolute dose rates are derived from them through multiplication by the average beta decay energy divided by the CSDA range for the maximum energy electron as indicated in

Equation (20). The scaled dose point kernels are relatively insensitive to these parameters. The use of these functions, therefore, allows improved dose estimates to be made easily by incorporating updated energy and range parameters when they become available.

The results of the calculation are also presented as dose distributions, in the same manner as Cross (2), in Tables 3 and 4. The calculations performed by Cross are based upon Spencer's electron transport monoenergetic dose point kernels. The dose distribution for yttrium-90 (⁹⁰Y) obtained using the Monte Carlo electron dose point kernels is compared with the earlier calculations by Cross (2) in Figure 9. The dose distribution calculated from the Monte Carlo kernels is 7% lower at the origin and is significantly higher for distances > 0.5 cm. This is illustrated in more detail in Figure 10, in which the ratio of the Monte Carlo curve to that obtained by Cross is shown as a function of distance. As indicated in Figure 10, the dose predicted by the Monte Carlo dose point kernels exceeds that predicted without straggling effects by almost a factor of three at 0.8 cm corresponding to 70% of the end point range. This behavior is expected on the basis of the comparison of the monoenergetic dose point kernels discussed previously.

As noted previously (2) experimentally observed doses exceed the values predicted by the Spencer dose

TABLE 2
Scaled Beta Dose Point Kernels

Scaled distance	³² P*	⁶⁷ Cu	⁹⁰ Y	¹³¹ I	¹⁸⁶ Re	¹⁸⁸ Re
0.00	0.2633E+01	0.2756E+02	0.2579E+01	0.3612E+02	0.9653E+01	0.9719E+01
0.04	0.2651E+01	0.1300E+02	0.2451E+01	0.1372E+02	0.6995E+01	0.8541E+01
0.08	0.2628E+01	0.9518E+01	0.2398E+01	0.8499E+01	0.6165E+01	0.8046E+01
0.12	0.2537E+01	0.7424E+01	0.2311E+01	0.5813E+01	0.5421E+01	0.7414E+01
0.16	0.2401E+01	0.5906E+01	0.2201E+01	0.4373E+01	0.4712E+01	0.6693E+01
0.20	0.2229E+01	0.4654E+01	0.2073E+01	0.3489E+01	0.4032E+01	0.5920E+01
0.24	0.2031E+01	0.3606E+01	0.1931E+01	0.2837E+01	0.3391E+01	0.5123E+01
0.28	0.1815E+01	0.2744E+01	0.1774E+01	0.2293E+01	0.2796E+01	0.4334E+01
0.32	0.1589E+01	0.2050E+01	0.1607E+01	0.1827E+01	0.2256E+01	0.3583E+01
0.36	0.1358E+01	0.1504E+01	0.1432E+01	0.1433E+01	0.1776E+01	0.2892E+01
0.40	0.1133E+01	0.1084E+01	0.1249E+01	0.1106E+01	0.1362E+01	0.2278E+01
0.44	0.9189E+00	0.7674E+00	0.1064E+01	0.8396E+00	0.1014E+01	0.1750E+01
0.48	0.7234E+00	0.5321E+00	0.8811E+00	0.6255E+00	0.7318E+00	0.1309E+01
0.52	0.5508E+00	0.3601E+00	0.7078E+00	0.4562E+00	0.5098E+00	0.9521E+00
0.56	0.4041E+00	0.2367E+00	0.5485E+00	0.3238E+00	0.3417E+00	0.6703E+00
0.60	0.2841E+00	0.1504E+00	0.4075E+00	0.2221E+00	0.2194E+00	0.4536E+00
0.64	0.1899E+00	0.9193E-01	0.2883E+00	0.1456E+00	0.1344E+00	0.2923E+00
0.68	0.1198E+00	0.5366E-01	0.1924E+00	0.9022E-01	0.7811E-01	0.1775E+00
0.72	0.7051E-01	0.2959E-01	0.1198E+00	0.5222E-01	0.4272E-01	0.1005E+00
0.76	0.3830E-01	0.1519E-01	0.6892E-01	0.2787E-01	0.2177E-01	0.5243E-01
0.80	0.1890E-01	0.7123E-02	0.3615E-01	0.1349E-01	0.1018E-01	0.2489E-01
0.84	0.8295E-02	0.2988E-02	0.1695E-01	0.5803E-02	0.4260E-02	0.1057E-01
0.88	0.3143E-02	0.1094E-02	0.6928E-02	0.2159E-02	0.1548E-02	0.3937E-02
0.92	0.9890E-03	0.3432E-03	0.2407E-02	0.6745E-03	0.4676E-03	0.1261E-02
0.96	0.2488E-03	0.9112E-04	0.6910E-03	0.1739E-03	0.1106E-03	0.3429E-03
1.00	0.5366E-04	0.2129E-04	0.1661E-03	0.3781E-04	0.2113E-04	0.8121E-04

* For convenience, the standard E format is used in this and following tables. The form aEn is to be interpreted as a · 10ⁿ.

TABLE 3
Calculated Beta Dose Distributions

³² P		⁶⁷ Cu		⁹⁰ Y	
R (g/cm ²)	r ² D(r) (mGy-cm ² /MBq-hr)	R (g/cm ²)	r ² D(r) (mGy-cm ² /MBq-hr)	R (g/cm ²)	r ² D(r) (mGy-cm ² /MBq-hr)
0.0000E+00	0.1008E+03	0.0000E+00	0.2829E+02	0.0000E+00	0.9798E+02
0.3323E-01	0.1015E+03	0.8592E-02	0.1617E+03	0.4520E-01	0.9312E+02
0.6646E-01	0.1006E+03	0.1718E-01	0.1250E+03	0.9041E-01	0.9114E+02
0.9970E-01	0.9715E+02	0.2578E-01	0.9690E+02	0.1356E+00	0.8781E+02
0.1329E+00	0.9192E+02	0.3437E-01	0.7422E+02	0.1808E+00	0.8364E+02
0.1662E+00	0.8534E+02	0.4296E-01	0.5575E+02	0.2260E+00	0.7879E+02
0.1994E+00	0.7777E+02	0.5155E-01	0.4092E+02	0.2712E+00	0.7336E+02
0.2326E+00	0.6951E+02	0.6014E-01	0.2936E+02	0.3164E+00	0.6743E+02
0.2659E+00	0.6083E+02	0.6874E-01	0.2064E+02	0.3616E+00	0.6108E+02
0.2991E+00	0.5201E+02	0.7733E-01	0.1427E+02	0.4068E+00	0.5440E+02
0.3323E+00	0.4337E+02	0.8592E-01	0.9767E+01	0.4520E+00	0.4746E+02
0.3656E+00	0.3519E+02	0.9451E-01	0.6640E+01	0.4972E+00	0.4041E+02
0.3988E+00	0.2770E+02	0.1031E+00	0.4483E+01	0.5424E+00	0.3348E+02
0.4320E+00	0.2109E+02	0.1117E+00	0.2988E+01	0.5877E+00	0.2690E+02
0.4652E+00	0.1547E+02	0.1203E+00	0.1948E+01	0.6329E+00	0.2084E+02
0.4985E+00	0.1088E+02	0.1289E+00	0.1231E+01	0.6781E+00	0.1549E+02
0.5317E+00	0.7272E+01	0.1375E+00	0.7494E+00	0.7233E+00	0.1095E+02
0.5649E+00	0.4585E+01	0.1461E+00	0.4362E+00	0.7685E+00	0.7309E+01
0.5982E+00	0.2700E+01	0.1547E+00	0.2401E+00	0.8137E+00	0.4553E+01
0.6314E+00	0.1467E+01	0.1632E+00	0.1232E+00	0.8589E+00	0.2619E+01
0.6646E+00	0.7237E+00	0.1718E+00	0.5774E-01	0.9041E+00	0.1374E+01
0.6979E+00	0.3176E+00	0.1804E+00	0.2422E-01	0.9493E+00	0.6440E+00
0.7311E+00	0.1203E+00	0.1890E+00	0.8867E-02	0.9945E+00	0.2633E+00
0.7643E+00	0.3787E-01	0.1976E+00	0.2782E-02	0.1040E+01	0.9145E-01
0.7976E+00	0.9528E-02	0.2062E+00	0.7386E-03	0.1085E+01	0.2626E-01
0.8308E+00	0.2054E-02	0.2148E+00	0.1725E-03	0.1130E+01	0.6310E-02

point kernels at large distances from the source. This trend is in qualitative agreement with the above result. Moreover, because of the area constraint given by Equation (8), such a trend requires that these values must be somewhat larger than the actual dose near the origin. Since the relative deviation is much smaller in this region, the effect could easily be masked by experimental uncertainties. A quantitative comparison has been made between data obtained for phosphorus-32 (³²P) by Clark et al. (15) and the calculated dose point kernels. Assuming 5% s.d. for the data, the reduced chi-square is 1.9 and 23.5 for the dose distributions calculated using the Monte Carlo kernels and the transport kernels respectively. As indicated in Figure 11, the comparison extends over almost two orders of magnitude in the dose distribution out to ~75% of the end-point range. Since the probability of observing a reduced chi-square greater than or equal to 1.9 for 12 degrees of freedom is only 3%, this result would indicate that the model used is not exactly appropriate. It would appear that there is some overestimation of the dose for the data corresponding to points far from the origin. In order to make the comparison, however, it was necessary to transform the data from an air to a water medium. Uncertainties in this transformation, together with uncertainties in the CSDA range lead to additional sources of error in the comparison not included in the

analysis. The average relative deviation between the data and the calculated curve is 7%. The maximum deviation is 17%, occurring at 0.61 cm.

Analytic Representation of Dose Point Kernels

Analytic representation of dose point kernels, as first suggested by Loevinger (16), provides a convenient means to perform dose estimation, circumventing the need for the storage of large data arrays, and for interpolating procedures. In this work we present functions which are entirely utilitarian in nature, chosen solely on the basis of their similarity in behaviour to the scaled beta dose point kernels. It should be emphasized that neither the functions nor the associated parameters used in the representations are connected with any basic physical mechanisms.

The function chosen to represent the bulk of the dose distribution was the three-parameter lognormal distribution given by

$$L(x) = \frac{1}{\sqrt{2\pi}\sigma(x_0 - x)} \exp - [(\log(x_0 - x) - \mu)^2 / 2\sigma^2]. \quad (24)$$

This function was selected because of its inherent convergence to zero at the controlled cut-off point, x_0 . The sharp upturn in the dose point kernels near the origin has been represented by two exponential functions both

TABLE 4
Calculated Beta Dose Distributions

¹³¹ I		¹⁸⁶ Re		¹⁸⁶ Re	
R (g/cm ²)	r ² D(r) (mGy-cm ² /MBq-hr)	R (g/cm ²)	r ² D(r) (mGy-cm ² /MBq-hr)	R (g/cm ²)	r ² D(r) (mGy-cm ² /MBq-hr)
0.0000E+00	0.2490E+03	0.0000E+00	0.1523E+03	0.0000E+00	0.1031E+03
0.1348E-01	0.1374E+03	0.1930E-01	0.1126E+03	0.4185E-01	0.9497E+02
0.2696E-01	0.1051E+03	0.3860E-01	0.1003E+03	0.8370E-01	0.9193E+02
0.4044E-01	0.8115E+02	0.5790E-01	0.8919E+02	0.1255E+00	0.8727E+02
0.5392E-01	0.6211E+02	0.7720E-01	0.7845E+02	0.1674E+00	0.8148E+02
0.6740E-01	0.4648E+02	0.9650E-01	0.6805E+02	0.2092E+00	0.7478E+02
0.8088E-01	0.3364E+02	0.1158E+00	0.5809E+02	0.2511E+00	0.6743E+02
0.9436E-01	0.2331E+02	0.1351E+00	0.4872E+02	0.2929E+00	0.5965E+02
0.1078E+00	0.1532E+02	0.1544E+00	0.4008E+02	0.3348E+00	0.5168E+02
0.1213E+00	0.9446E+01	0.1737E+00	0.3227E+02	0.3766E+00	0.4379E+02
0.1348E+00	0.5401E+01	0.1930E+00	0.2535E+02	0.4185E+00	0.3619E+02
0.1483E+00	0.2818E+01	0.2123E+00	0.1940E+02	0.4603E+00	0.2910E+02
0.1618E+00	0.1318E+01	0.2316E+00	0.1441E+02	0.5022E+00	0.2271E+02
0.1752E+00	0.5450E+00	0.2509E+00	0.1037E+02	0.5440E+00	0.1714E+02
0.1887E+00	0.2009E+00	0.2702E+00	0.7190E+01	0.5859E+00	0.1246E+02
0.2022E+00	0.7169E-01	0.2895E+00	0.4785E+01	0.6277E+00	0.8674E+01
0.2157E+00	0.2970E-01	0.3088E+00	0.3035E+01	0.6696E+00	0.5740E+01
0.2292E+00	0.1537E-01	0.3281E+00	0.1822E+01	0.7114E+00	0.3582E+01
0.2426E+00	0.8548E-02	0.3474E+00	0.1024E+01	0.7533E+00	0.2088E+01
0.2561E+00	0.4517E-02	0.3667E+00	0.5330E+00	0.7951E+00	0.1125E+01
0.2696E+00	0.2186E-02	0.3860E+00	0.2525E+00	0.8370E+00	0.5526E+00
0.2831E+00	0.9401E-03	0.4053E+00	0.1064E+00	0.8788E+00	0.2429E+00
0.2966E+00	0.3497E-03	0.4246E+00	0.3875E-01	0.9207E+00	0.9334E-01
0.3100E+00	0.1093E-03	0.4439E+00	0.1172E-01	0.9625E+00	0.3056E-01
0.3235E+00	0.2817E-04	0.4632E+00	0.2773E-02	0.1004E+01	0.8350E-02
0.3370E+00	0.6126E-05	0.4825E+00	0.5301E-03	0.1046E+01	0.1985E-02

of which become completely negligible in the far region. In addition, a small step function, terminating at $x = 1$, was found to improve the fit near this region. The form of the scaled dose point kernel for an individual beta group can then be written

$$F_{\beta}(x) = aL(x) + b_1 \exp(-\lambda_1 x) + b_2 \exp(-\lambda_2 x) + CII(x), \quad (25)$$

where

$$\begin{aligned} \Pi(x) &= 1, 0 \leq x \leq 1 \\ &= 0, x > 1. \end{aligned} \quad (26)$$

The parameters were found by nonlinear least squares fitting based on the Levenberg-Marquardt algorithm (17). The parameters found by this method are listed in Table 5. The quality of the fits are illustrated in Figures 12 and 13. The average deviation over the range $0 \leq x \leq 1$ for all radionuclides treated is 2%.

CONCLUSIONS

Beta dose point kernels have been calculated for six radionuclides potentially important for radioimmunotherapy. The inclusion of straggling effects leads to improved agreement with experimental results for ³²P, and leads to significantly increased dose estimates at

distances greater than approximately three-quarters of the CSDA range. A satisfactory analytic representation of the scaled dose point kernels for individual beta groups has been obtained. The model used consists of a lognormal function together with two short range exponential functions and a small contribution from a step function.

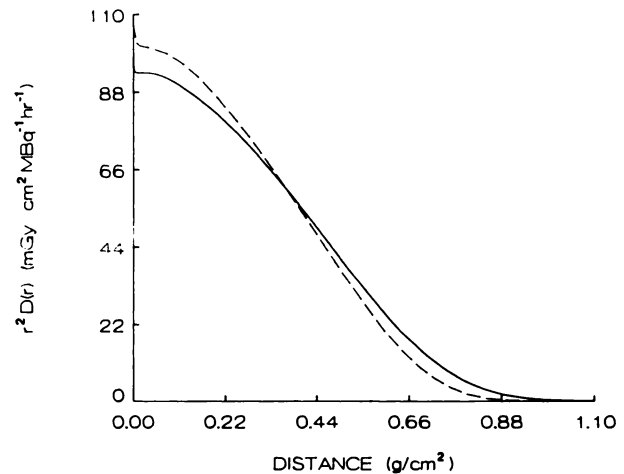


FIGURE 9
Comparison between the beta dose distribution for ⁹⁰Y calculated using the transport kernels (---) and the Monte Carlo kernels (—).

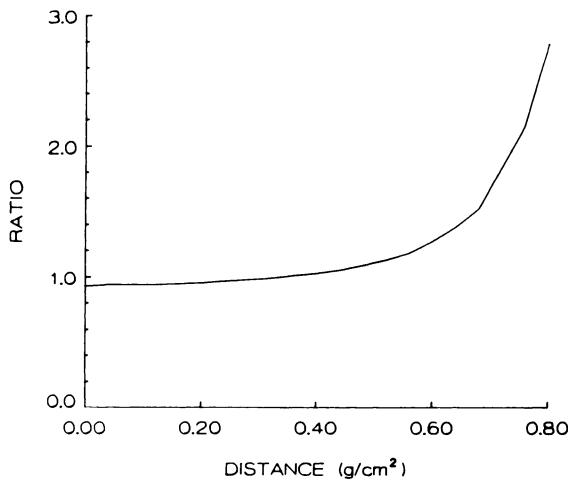


FIGURE 10
The ratio of the transport to the Monte Carlo ^{90}Y data of Figure 9, illustrating the slight overestimation at the origin and significant underestimation at large distances by the former.

ACKNOWLEDGMENTS

The authors thank the Natural Sciences and Engineering Research Council of Canada and the Province of Ontario for financial assistance.

APPENDIX

Calculation of Allowed Beta Spectra

The expression for the beta spectrum of an allowed transition with end-point energy E_i may be written (11)

$$n_i(E) = CF(Z, W_s) p_s W_s (E_i - E)^2 \quad (\text{A1})$$

In the above expression C is a normalizing constant, $F(Z, W_s)$ is the Fermi function where Z is the atomic number of the

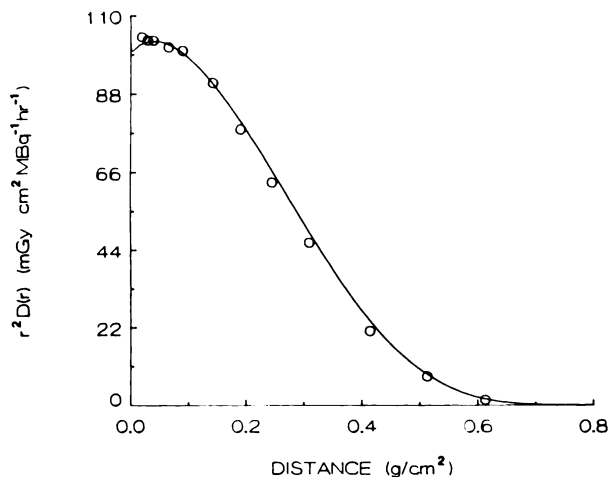


FIGURE 11
Comparison between the ^{32}P dose distribution calculated on the basis of the Monte Carlo dose point kernels (solid line) and experimental results (open circles).

daughter nucleus, and p_s and W_s are the screened momentum and total energy, respectively. These satisfy the relations

$$p_s = \sqrt{W_s^2 - m_e^2 c^4} \quad (\text{A2})$$

and

$$W_s = E + m_e c^2 - V_0, \quad (\text{A3})$$

where V_0 is a screening potential and $m_e c^2$ is the electron rest mass energy. In this work the screening potential has been calculated as

$$V_0 = 30.77 Z^{4/3} \text{ eV}. \quad (\text{A4})$$

The Fermi function has been calculated using the Bethe Bacher approximation (18) modified by us for $Z > 50$. Introducing the relativistic quantities

$$\omega = W/m_e c^2 \quad (\text{A5})$$

and

$$\eta = p/m_e c \quad (\text{A6})$$

the approximation is

$$F(Z, W) = F_N(Z, W) [\alpha^2 Z^2 \omega^2 + (\omega^2 - 1)/4]^S \quad (\text{A7})$$

where α is the fine structure constant, 137^{-1} , and

$$S = \sqrt{1 - \alpha^2 Z^2} - 1. \quad (\text{A8})$$

The first term in Equation (A7) is the nonrelativistic Fermi function given by

$$F_N(Z, W) = 2\pi\nu/(1 - e^{-2\pi\nu}) \quad (\text{A9})$$

with

$$\nu = \alpha Z \omega/\eta. \quad (\text{A10})$$

The Bethe Bacher approximation yields values well within 0.5% for $Z \leq 50$, but becomes less accurate for large Z . We have developed a correction factor of the form

$$C = 1 + [a(Z - 50) + b(Z - 50)^2] (1 - \exp(-c\nu)), \quad (\text{A11})$$

with

$$a = 4.05 \times 10^{-4}$$

$$b = 2.23 \times 10^{-5}$$

$$c = 1.26.$$

As an example of the quality of the approximation of Equation (A11), the values yielded for T for the momentum range $0 \leq \eta \leq 4.9$ exhibit a maximum discrepancy of 0.45%. Without the correction factor the maximum discrepancy for this case is 3.4%.

Calculation of First-Forbidden Shape Factor

For first-forbidden unique transitions the spectrum is further modified by an additional shape factor. This quantity may be written

$$S = L_0 \cdot (\omega_i - \omega)^2 + 9L_1, \quad (\text{A12})$$

where ω_i is the total relativistic energy at the end point and L_0 and L_1 are tabulated functions (12) of the relativistic electron

TABLE 5
Parameters for Analytic Representation of Scaled Dose Point Kernels

Nuclide	Energy (MeV)	A	X ₀	μ	σ	b ₁	λ ₁	b ₂	λ ₂	Constant
³² P	1.708	4.36	1.3253	0.5066	0.3248	-0.583	8.967	0.038	2784.921	7.21E-05
⁶⁷ Cu	0.184	3290.20	1.2436	2.1525	0.5594	2.377	25.480	1.852	157.690	9.42E-06
	0.395	115.15	1.2356	1.3441	0.4730	1.127	30.716	1.192	280.276	9.38E-06
	0.484	55.16	1.2414	1.1564	0.4467	0.836	35.453	0.991	358.132	9.68E-06
	0.577	30.68	1.2533	1.0051	0.4210	0.618	44.193	0.819	461.127	9.32E-06
⁹⁰ Y	2.286	3.12	1.2655	0.4020	0.3577	0.113	1161.102	—	—	6.69E-05
¹³¹ I	0.248	1940.70	1.2289	2.0483	0.5564	2.238	25.449	1.864	187.985	8.79E-06
	0.304	708.36	1.2252	1.8071	0.5325	1.913	26.092	1.730	214.525	8.72E-06
	0.334	454.22	1.2239	1.6987	0.5211	1.760	26.495	1.641	227.646	8.78E-06
	0.606	40.71	1.2425	1.0825	0.4373	0.845	35.316	1.029	411.509	9.15E-06
	0.807	6.22	1.2766	0.6122	0.3625	0.820	24.472	0.835	434.741	1.13E-05
¹⁸⁶ Re	0.934	17.81	1.2519	0.8738	0.4076	0.467	58.020	0.657	651.510	5.79E-06
	1.072	12.63	1.2593	0.7852	0.3924	0.342	75.940	0.505	714.958	2.33E-06
¹⁸⁸ Re	1.487	6.03	1.2960	0.5981	0.3491	-0.087	0.002	0.374	597.771	8.68E-02
	1.965	3.85	1.3409	0.4958	0.3157	-0.031	6.354	0.157	1658.212	5.90E-05
	2.120	3.49	1.3549	0.4762	0.3076	-0.028	6.281	0.113	2546.797	5.84E-05

momentum. We have approximated these functions by

$$L_0 = a_0 + b_0\eta, \quad (A13)$$

where

$$a_0 = 0.997834 + Z(1.1975 \cdot 10^{-4} - Z(1.85 \cdot 10^{-5}))$$

$$b_0 = 4.555 \cdot 10^{-4} - Z(1.562 \cdot 10^{-4} + Z(1.0165 \cdot 10^{-6}))$$

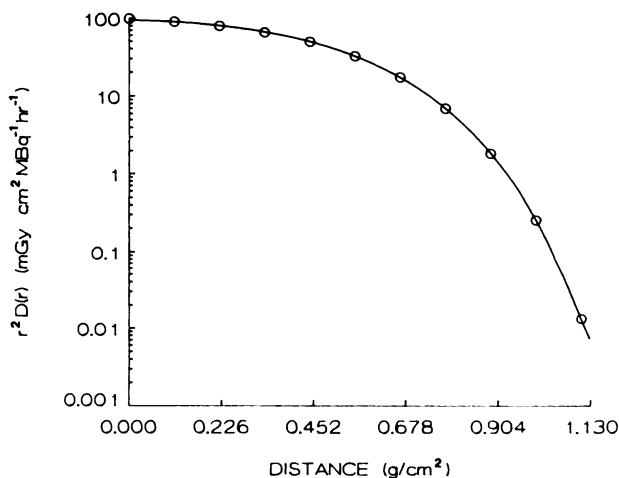


FIGURE 12
The quality of the analytic representation (—) of the calculated ⁹⁰Y beta dose distribution. Circles are values from Table 3.

and

$$L_1 = (c + d\eta + fe^{-\lambda_1\eta} + ge^{-\lambda_2\eta}) \eta^2, \quad (A14)$$

where

$$c = 0.111235 - (2.6377 \cdot 10^{-5}) Z - (8.738 \cdot 10^{-6}) Z^2 + (2.204 \cdot 10^{-8}) Z^3$$

$$d = 2.8789 \cdot 10^{-5} - (1.146 \cdot 10^{-5}) Z + (4.483 \cdot 10^{-7}) Z^2 - (6.1 \cdot 10^{-10}) Z^3$$

$$f = 9.55727 (1 - \exp(-3.81 \cdot 10^{-4} Z^2))$$

$$g = 0.56731 (1 - \exp(-4.15 \cdot 10^{-4} Z^2))$$

$$\lambda_1 = 20.0641$$

$$\lambda_2 = 4.878 - (4.166 \cdot 10^{-3}) Z.$$

Calculation of CSDA Range

For electron energies between 50 eV and 500 eV, the CSDA range in water was calculated as

$$r_1 = a_1 + b_1E + c_1E^2 + d_1E^3, \quad (A15)$$

where E is the energy in eV with

$$a_1 = 0.945387 \cdot 10^{-6}$$

$$b_1 = 0.005286 \cdot 10^{-6}$$

$$c_1 = -2.1207 \cdot 10^{-12}$$

$$d_1 = 3.0 \cdot 10^{-15}.$$

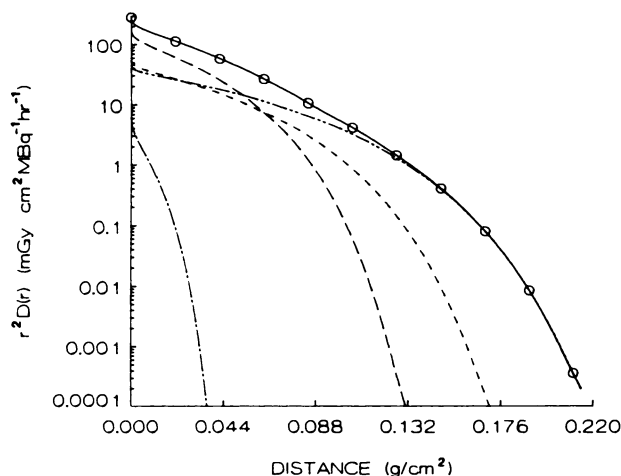


FIGURE 13
Analytic representation of the beta dose distribution for ^{67}Cu . Also shown are the contributions from the individual beta groups of which this spectrum is composed. These occur at energies of 0.1835 MeV (---), 0.395 MeV (— —) 0.484 MeV (— — —), and 0.577 MeV (— — — —). The solid line represents the sum of the above contributions, while the circles correspond to the values in Table 3.

For electron energies between 1 and 10 keV the range was calculated as

$$r_2 = a_2 + b_2 E + c_2 E^2 \quad (\text{A16})$$

with

$$a_2 = -1.33941 \cdot 10^{-6}$$

$$b_2 = 0.006123 \cdot 10^{-6}$$

$$c_2 = 2.0414 \cdot 10^{-12}$$

In the region from 500 to 1,000 eV, the weighted average

$$r = (E - 500) r_2/500 + (1000 - E) r_1/500 \quad (\text{A17})$$

was used.

Finally, for $E > 10$ keV, the form is

$$\ln r = a + b \ln E + c(\ln E)^2 + d(\ln E)^3 \quad (\text{A18})$$

with E in MeV and

$$a = -0.814245$$

$$b = 1.24742$$

$$c = -0.130086$$

$$d = -0.010436$$

The range is given in g cm^{-2} for all the above.

REFERENCES

1. Larson SM, Carrasquillo JA, Reynolds JC, et al. Therapeutic applications of radiolabelled antibodies: cur-

- rent situations and prospects. *Nucl Med Biol* 1986; 13:207-213.
2. Cross WG, Ing H, Freedman NO, Mainville J. Tables of beta ray dose distributions in water, air and other media. Chalk River, Ontario: Atomic Energy of Canada Ltd., Chalk River Nuclear Laboratories. 1982; AECL-7617.
3. Spencer LV. Energy dissipation by fast electrons. Monograph No. 1 1959; National Bureau of Standards.
4. Berger MJ. Monte Carlo calculation of the penetration of diffusion of fast charged particles. In: Alder B, Fernbach S, Rotenberg M, eds. *Methods in computational physics*. New York: Academic Press, 1963: 135-215.
5. Berger MJ. Improved point kernels for electron and beta ray dosimetry. Washington, DC: US Department of Commerce, National Bureau of Standards 1973; NBSIR 73-107.
6. Berger MJ. Distribution of absorbed dose around point sources of electrons and beta particles in water and other media. *MIRD Pamphlet No. 7. J Nucl Med* 1971; 12 (suppl. 5):7-23.
7. Dierckx P. A fast algorithm for smoothing data on a rectangular grid while using spline functions. *SIAM J Numer Anal* 1982; 19:1286-1304.
8. Prestwich WV, Chan LB, Kwok CS, Wilson BC. Dose point kernels for beta-emitting radioisotopes. In: Proceedings of the Fourth International Radiopharmaceutical Dosimetry Symposium in Oak Ridge, TN, USA, Nov. 5-8 1985; 545:561.
9. Berger MJ, Seltzer SM. Stopping powers and ranges of electrons and positrons. 2nd ed. Washington DC: US Department of Commerce, National Bureau of Standards. NBSIR, 1982; 82-2550-A.
10. LaVerne JA, Mozumder A. Effect of phase on the stopping and range distribution of low-energy electrons in water. *J Phys Chem* 1986; 90:3242-3247.
11. Dillman LT. Radionuclide decay schemes and nuclear parameters for use in radiation-dose estimation. *MIRD Pamphlet No. 4. J Nucl Med* 1969; 10 (suppl 2):5-32.
12. Siegbahn K. Beta and gamma ray spectroscopy. Chap. 14. Amsterdam: North-Holland Publishing, 1955.
13. Radionuclide transformation energy and intensity of emissions. In: Sowby FD, ed. *Annals of the ICRP, ICRP Publication 38*. Vol. 11-13. Pergamon Press, 1983.
14. Lederer CM, Shirley VS. Table of isotopes. Seventh ed. New York: John Wiley, 1978.
15. Clark RK, Brar SS, Marinelli LD. Ionization of air by beta rays from point sources. *Radiology* 1955; 64:94-104.
16. Loevinger R. The dosimetry of beta sources in tissue. The point source function. *Radiology* 1956; 66:55-62.
17. Marquardt DW. An algorithm for least squares estimation of non-linear parameters. *J Soc Indust Appl Math* 1963; 11:431-441.
18. Bethe HB, Bacher RF. Nuclear Physics A. Stationary states of nuclei. *Rev Mod Phys* 1936; 8:82-229.